Development of Redox-Active Optical Mesostructures at Chemically Modified Electrode Interfaces

Ying Wu, Brian W. Pfennig, and Andrew B. Bocarsly*

Department of Chemistry, Frick Laboratory, Princeton University, Princeton, New Jersey 08544-1009

Edward P. Vicenzi

Princeton Materials Institute, Bowen Hall, Princeton, New Jersey 08540-5211

Received December 21, 1994[⊗]

Polymeric films of $[Fe^{II}(CN)_6-Pt^{IV}(NH_3)_4]_n$ were prepared on optically transparent indium tin oxide (ITO) electrode surfaces via oxidative polymerization of the monomer $[Pt(NH_3)_4]_2[(NC)_5Fe-CN-Pt(NH_3)_4-NC-Fe(CN)_5]$. Irradiation at 457 nm into the intervalence charge transfer band of the interfacial polymer causes the cleavage of bridging -CN- to Pt bonds, leading to the dissociation of polymeric film into shorter-chain $[Fe-Pt]_n$ oligomers, $[Pt(NH_3)_4]^{2+}$ and $[Fe(CN)_6]^{3-}$. When photolysis is carried out with the modified interface immersed in an aqueous solution containing transition metal cations M^{n+} ($M^{n+} = Ni^{2+}$, Fe^{2+}, Mn^{2+}, Cr^{3+}), M^{n+} reacts with photogenerated $[Fe(CN)_6]^{3-}$ complexes to form mixed metal cyanometalates of the form $[M-NC-Fe(CN)_5]^{2-}$ on the electrode surface. As a result, M^{n+} is incorporated into the interfacial lattice only at the irradiated regions. The film after M^{n+} incorporation is different in color compared to the original $[Fe-Pt]_n$ polymer film. Images may be developed on such a film by irradiating the sample through a mask. In this paper we report the formation and characterization of such multicomponent electrode surfaces. In addition, the potential applicability of these multicomponent electrodes as molecular electronic devices is discussed.

Introduction

Recent development in the area of chemically modified electrodes has brought about the need for high-resolution spatial control of structures with multicomponent, redox-active polymeric films.[1-5] Such control is desirable in the dimension perpendicular to the electrode surface (overlayer structures) as well as parallel to the electrode surface (lateral domains). Recently, several experimental techniques[6-8] involving multiple electrochemical/photochemical steps have been developed. One particular area of interest in these redox-active polymer films relates to pattern formation on electrode surfaces, especially when electrochromic materials are incorporated. Electrochromism allows for more dynamic systems that may prove useful as light-modulating or light-sensing devices.

Our group has focused on the surface-attached mixed metal cyanometalates which are structurally similar to Prussian blue (PB). They can be readily derivatized onto a number of different electrode surfaces through anodic processes, and their robust chemical nature makes them good candidates for the fabrication of electrode surfaces with potential applications in areas such as molecular electronics, photochemical energy conversion, display and memory devices, electrocatalysis, and sensors.

The system reported here is based on the unique electrochemical and photochemical properties of the trinuclear complex $[Pt(NH_3)_4]_2[(NC)_5Fe-CN-Pt(NH_3)_4-NC-Fe(CN)_5]$ (**A**),[9] where there exists a photoinduced ($\lambda_{max} = 424$ nm) intervalence charge transfer (IT) process that is two-electron in nature and involves all three metal centers.[10] In addition, this complex readily undergoes oxidative polymerization on a variety of electrode surfaces. For the purpose of fabricating optical devices, the transparent indium tin oxide (ITO) electrode is most suitable. The oxidative polymerization mechanism is outlined as follows (ligands are omitted for clarity).

$$n[Fe^{II}-Pt^{IV}-Fe^{II}] \xrightarrow{[ox]} n[Fe^{III}-Pt^{IV}-Fe^{III}] \xrightarrow{n Pt^{II}} [Fe^{II}-Pt^{IV}]_{2n} \quad (1)$$

$$2[Fe^{II}-Pt^{IV}]_n \xrightarrow{[ox]} 2[Fe^{III}-Pt^{IV}]_n \xrightarrow{Pt^{II}} [Fe^{II}-Pt^{IV}]_{2n+1} \quad (2)$$

Bridging from the cyanide ligands to the Pt centers may take place in one, two, or three dimensions due to the octahedral geometry of the complex. This gives rise to one-dimensional, sheet, and network polymer systems. The previously mentioned IT transition of the trinuclear monomer results in the simultaneous oxidation of Fe centers from 2+ to 3+ and the reduction of Pt from 4+ to 2+, during which process the linkage of bridging -CN- ligand to Pt is broken. This photodissociation may be preserved in polymer films generated at strategically chosen derivatizing potentials. Based on known photochemistry of the monomer,[10] it is reasonable to assume the following.

$$[Fe^{II}-Pt^{IV}]_{2n+1} \xrightarrow{h\nu} 2[Fe^{III}-Pt^{IV}]_n + [Pt(NH_3)_4]^{2+} \quad (3)$$

$$[Fe^{II}-Pt^{IV}]_n \xrightarrow{h\nu} n[Fe(CN)_6]^{3-} + n[Pt(NH_3)_4]^{2+} \quad (4)$$

The procedures used to generate multicomponent electrode surfaces are illustrated in Scheme 1. The $[Fe-Pt]_n$ polymer film is first laid down on an ITO surface electrochemically and

[⊗] Abstract published in *Advance ACS Abstracts*, July 1, 1995.

(1) Wrighton, M. S. *Science* **1986**, *231*, 32–37.
(2) Chidsey, C. E.; Murray, R. W. *Science* **1986**, *231*, 25–31.
(3) Murray, R. W.; Ewing, A. G.; Durst, R. A. *Anal. Chem.* **1987**, *59*, 379A–399A.
(4) Natan, M. J.; Wrighton, M. S. *Prog. Inorg. Chem.* **1989**, *37*, 391–494.
(5) Ryan, M. D.; Bowden, E. F.; Chambers, J. Q. *Anal. Chem.* **1994**, *66*, 360R–427R.
(6) Gould, S.; Gray, K. H.; Linton, R. W.; Meyer, T. J. *Inorg. Chem.* **1992**, *31*, 5521–5525.
(7) Callomb-Dunand-Sauthier, M.-N.; Doronzier, A.; Ziessel, R. *J. Phys. Chem.* **1993**, *97*, 5973–5979.
(8) Gould, S.; O'Toole, T. R.; Meyer, T. J. *J. Am. Chem. Soc.* **1990**, *112*, 9490–9496.
(9) Pfennig, B. W.; Bocarsly, A. B. *Coord. Chem. Rev.* **1991**, *111*, 91–96.
(10) Pfennig, B. W.; Bocarsly, A. B. *J. Phys. Chem.* **1992**, *96*, 226–233.

0020-1669/95/1334-4262$09.00/0

Scheme 1

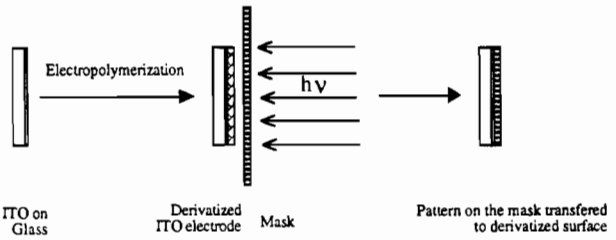

then irradiated in a transition metal cation containing solution through a mask. After photolysis, the $[Fe-Pt]_n$ polymer film constitutes one component on the surface (in the masked regions), and the mixed metal cyanometalate formed from the photoproduct ferricyanide and the transition metal cations dissolved in solution makes up the second component (in the photolyzed regions). A multicomponent surface mesostructure with lateral spatial control is thus constructed. The photochemical step directly generates the second desired component on the surface; no follow-up chemistry is required.

Among the possible applications of such a multicomponent electrode is the fabrication of an optoelectronic diffraction grating. The desired system starts with an electrode with stripe structures of alternating colors across the surface, one color being that of the $[Pt-Fe]_n$ polymer and the other being the color of the photochemically generated cyanometalate. If the cyanometalate is electrochromic and its absorbance can be changed to an absorbance similar to that of $[Fe-Pt]_n$ polymer film, then by varying the applied potential the absorbance of the cyanometalate may be changed to match the $[Fe-Pt]_n$ absorbance so that the stripes become invisible on the electrode surface at some specific electrode potential (or potential range). Due to the electrochromic property of the chosen cyanometalate, the above process should be reversible, i.e., the uniformly colored surface may be changed back to the striped state by simply changing the potential so that the electrochromic cyanometalate reverts back to its original color. We dub such an electrode a "venetian blind" electrode because the switching between a striped surface and a uniformly colored surface is analogous to the opening and closing of a venetian blind. In addition, when the width of the stripes is small enough, this "molecular venetian blind" also becomes a potential-controlled diffraction grating. That is, the grating is "on" when the electrode is in the striped state and "off" when the surface is in the uniformly colored state.

We report here the preparation of several cyanometalate-based multicomponent polymer film electrodes with controlled lateral mesostructure. The electrochemical and photochemical properties of this class of electrodes will be discussed.

Experimental Section

Materials. Optically transparent indium tin oxide slides (ITO) were obtained from Delta Technologies Inc. Potassium ferricyanide (Fisher) and tetraamineplatinum(II) nitrate (Aldrich) were used without further purification. Ronchi rulings (50 lines per inch, and 300 lines per inch) used as masks in photolysis were obtained from Edmund Scientific.

Instrumentation. All electrochemical studies were performed on a Princeton Applied Research (PAR) Model 263 potentiostat equipped with a PC workstation running on PAR 270 electrochemistry software. A standard one-compartment, three-electrode cell was employed, with a large-area Pt foil as counter electrode and a saturated calomel electrode (SCE) as reference. Laser irradiation of the electrode surface was performed using a Coherent Innova 70 argon ion laser emitting at 457 nm. A Ronchi Ruling was held adjacent to the nonconducting side of the ITO slide. This assembly was immersed in an aqueous solution and irradiated from the Ronchi ruling side with the laser beam perpendicular to the surface of the electrode. A typical photolysis lasted 30–45 min. The laser power output was kept at ~30 mW/cm^2 with an expanded beam of 1 in. in diameter. Light intensities were measured using a Newport Research Model 815 power meter. Absorption spectra were recorded on an HP 8450 diode array UV–vis absorption spectrometer. FTIR data were obtained on a Nicolet Model 800 FTIR spectrophotometer equipped with a diffuse-reflectance IR-PLAN Infrared Microscope Accessory station from Spectra Tech Inc. All IR spectra were referenced against a standard gold film on single-crystal silicon substrate. The area sampled under the microscope was typically 200 × 200 μm^2.

Electron Probe Microanalysis. Electron probe microanalysis (EPMA) was performed with a CAMECA SX-50. The EPMA method employs a primary beam of focused electrons which cause target atoms to reach an excited state via inner-shell electron ionization. During relaxation, X-rays characteristic of the target atoms are emitted. High spectral resolution X-ray measurements are made using crystal monochromators and gas-flow X-ray detectors. Analyses were performed using an accelerating voltage of 15 kV and a regulated beam current of 20 nA. Both secondary and backscattered electron images were used to locate areas suitable for analysis. The spatial resolution for a point analysis is approximately 1 μm^3 for the above instrumental conditions; hence, both the polymeric film and the ITO electrode were part of the activation volume.

Electrodes were mounted using double-sided carbon tape followed by deposition of a thin film of carbon (~200 Å in thickness) to ensure proper electrical grounding to the instrument. Standard materials used to calibrate X-ray lines of interest are as follows: O Kα (Al_2O_3), Na Kα ($NaAlSi_3O_8$), Mg Kα (MgO), Si Kα ($CaSiO_3$), K Kα ($KAlSi_3O_8$), Cr Kα ($FeCr_2O_4$), Mn Kα ($Mn_3Al_2Si_3O_{12}$), Fe Kα (Fe_2O_3), Ni Kα (Ni), In Lα (InP), Sn Lα (SnO_2), and Pt Mα (Pt). No attempt was made to analyze for N or C in this data set, and H is not detectable by EPMA. Peak and background intensities were measured for 20 and 10 s, respectively. On-line matrix corrections were performed using the PAP version of the $\Phi(\rho Z)$ method[11,12] with a SUN IPX workstation computer.

Results and Discussion

Electropolymerization. The trinuclear complexes $[Pt(NH_3)_4]_2[(NC)_5Fe-CN-Pt(NH_3)_4-NC-Fe(CN)_5]$ and $Na_4[(NC)_5Fe-CN-Pt(NH_3)_4-NC-Fe(CN)_5]$ were prepared according to literature procedures.[13] The Fe centers can be easily oxidized at the ITO surface, giving rise to $[Fe^{III}-Pt^{IV}-Fe^{III}]^{2-}$ species, which can further oxidize $[Pt(NH_3)_4]^{2+}$, when it is present in solution, to form polymers consisting of repeating $[Fe^{II}(CN)_6-Pt^{IV}(NH_3)_4]$ units (eqs 1 and 2). Typically, the solution used for polymerization contained 5 mM $[Fe-Pt-Fe]^{4-}$ complex and 5 mM $[Pt(NH_3)_4]^{2+}$ complex in a 0.1 M $NaNO_3$ supporting electrolyte solution. The ITO working electrodes were rinsed with dilute HCl, followed by distilled water, wiped dry, and then derivatized for 1–5 min. The electrodes were dried in air, rinsed with distilled water, and dried again before cyclic voltammetric analysis was carried out in 0.5 M $NaNO_3$ electrolyte solutions. Typical surface coverage is in the range of $(1.0-2.5) \times 10^{-8}$ mol/cm^2.

Control of Polymerization by Derivatizing Potential. The cyclic voltammogram of a film first derivatized at 1.4 V vs SCE is shown in Figure 1a. Four sets of waves are present although the $[Fe-Pt-Fe]^{4-}$ in solution yields only one set of two-electron peaks at 0.54 V vs SCE. The increased number of peaks found in the cyclic voltammogram of the polymer-modified surface is indicative of an increased ratio of bridging cyanides to Fe centers.[14] The $Fe^{III/II}$ redox potential of cyanometalates is strongly dependent on the number of bridging -CN- ligands

(11) Pouchou, J. L.; Pichoir, F. *Rech. Aerosp.* **1984**, *5*, 349–367.
(12) Pouchou, J. L.; Pichoir, F. M. A. *Microbeam Anal.* **1988**, *23*, 315–318.
(13) Zhou, M.; Pfennig, B. W.; Steiger, J.; Van Engen, D.; Bocarsly, A. B. *Inorg. Chem.* **1990**, *29*, 2457–2460.
(14) Pfennig, B. W.; Bocarsly, A. B. *Inorg. Chem.* **1991**, *30*, 666–672.

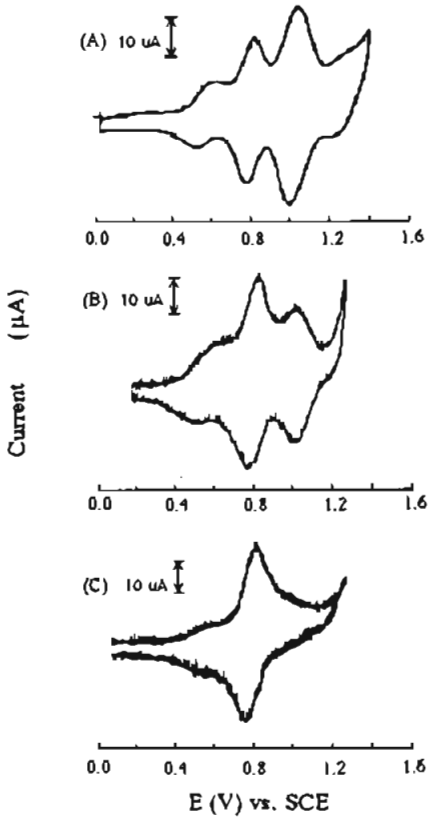

Figure 1. Cyclic voltammograms of $[Fe-Pt]_n$ polymer films derivatized at different anodic potentials: electrolyte used, 0.5 M $NaNO_3$; scan rate, 20 mV/s. Derivatizing potential: (A) E = 1.4 V vs SCE; (B) E=1.0 V vs SCE; (C) E = 0.7 V vs SCE.

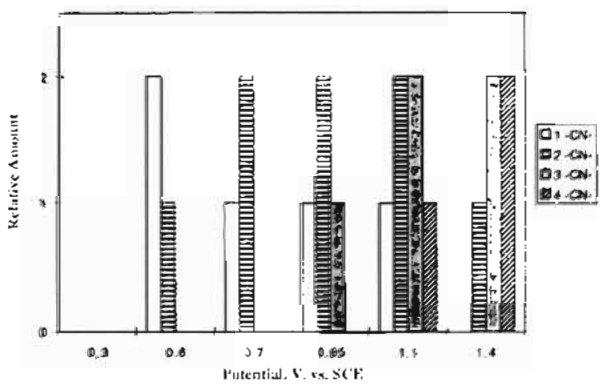

Figure 2. Relative amount of various Fe centers as a function of derivatizing potential. Derivatizing time was held constant at 45 s.

associated with a particular Fe center. From a molecular orbital point of view, the formation of a CN−Pt bond is expected to stabilize the CN π^*-orbital, giving rise to a lower-energy t_{2g} orbital set on ferrocyanide. As a result, the redox potential of the Fe centers shifts positive. On the basis of these facts, the waves at 0.54, 0.82, 1.05, and 1.27 V vs SCE are assigned to the redox events of Fe centers with one, two, three, and four bridging cyanide ligands, respectively.

To further confirm the assignment of these waves, a systematic investigation of the effect of derivatizing potential was performed. A separate experiment in which 45 s derivatization times were employed while the derivatization potential of the electrodes was varied yields the results shown in Figure 2. The relative amount, which is expressed in terms of the smallest integer ratio, of Fe centers with various numbers of bridging CN ligands was obtained by integrating the cyclic voltammetric peaks taken in 1.0 M $NaNO_3$ supporting electrolyte solution. Derivatization at 0.3 V vs SCE leads to no cyclic voltammetric peaks since no Fe centers can be oxidized at this potential and thus no polymerization occurred at the electrode surface. When the applied potential is shifted positive to 0.6 V vs SCE, two cyclic voltammetric peaks are observed (0.56 and 0.82 V vs SCE), the first corresponding to singly-bridged ferrocyanide and the second corresponding to the doubly-bridged species. As the applied potential is made more positive than that at the second peak, a third CV peak at 1.05 V vs SCE appears. At this derivatization potential, both singly- and doubly-bridged Fe centers can be oxidized and reacted with additional Pt(II) to form more highly bridged oligomers. At potentials more positive than that at the third peak, the resulting ITO electrodes show a fourth CV response as expected.

In short, the dependence of the $Fe^{(I)/(I)}$ redox potential on the number of bridging cyanides offers a means to control the degree of cross-linking in the polymer through the control of the potential applied to the working ITO electrode, since a more highly cross-linked system requires a more positive potential to keep the polymerization process going. The cyclic voltammograms of electrodes derivatized at 1.0 and 0.7 V vs SCE are shown in parts B and C, respectively, of Figure 1. At 0.7 V, the majority of the Fe centers on the electrode surface have two bridging cyanides. Therefore, the polymers formed must be mostly one dimensional. At 1.0 V vs SCE, the resulting film contains almost equal amounts of Fe center with two or three bridging CN ligands. The more extensive bridging allows for the generation of two- or even three-dimensional structures, leading to a polymeric film of reasonable thickness.

Photochemical Patterning of the Interface. Photolysis experiments performed on dry films revealed that films derivatized at 1.4 V vs SCE were photochemically inactive. In this case, the high degree of cross-linking is likely to allow for a high degree of bond reformation due to the limited degree of freedom. On the other hand, a derivatizing potential of less than 0.7 V vs SCE was found to be inadequate to give rise to enough cross-linking to produce an interfacial layer of sufficient thickness for light-modulating purposes, even though there is enough material on the electrode surface for cyclic voltammetric analysis. An intermediate potential of 1.0 V vs SCE was found to be suitable for generating a polymeric film of good stability and reasonable thickness while preserving the photodissociation properties of the monomeric unit. Thus, the photochemical patterning discussed below was performed on electrodes modified at 1.0 V vs SCE.

As shown in Scheme 1, by using a mask, selected areas of the electrode surface can be photolyzed. The film in the irradiated areas undergoes cleavage of the N−Pt bond (eq 3). When the electrode is irradiated in a solution of 0.1 M $NaNO_3$, both photoproducts, $[Pt(NH_3)_4]^{2+}$ and $[Fe(CN)_6]^{3-}$, dissolve in the solution, undermining the structural integrity of the film and eventually leading to the complete dissolution of the film in the irradiated area. This was demonstrated by IR spectroscopy (Figure 3). Microscopic diffuse reflectance FTIR spectra were recorded for the two regions on the electrode surface separately by narrowing the view window on the microscope to within a specific stripe. The photomasked areas show prominent peaks in the cyanide stretching frequency range, indicating that the $[Fe-Pt]_n$ polymer network is still intact. On the other hand, the irradiated area does not have any observable IR transitions in the corresponding wavelength region. Further, when the electrode was examined using an optical microscope, only the light blue color of the ITO film was observed in the photolyzed regions.

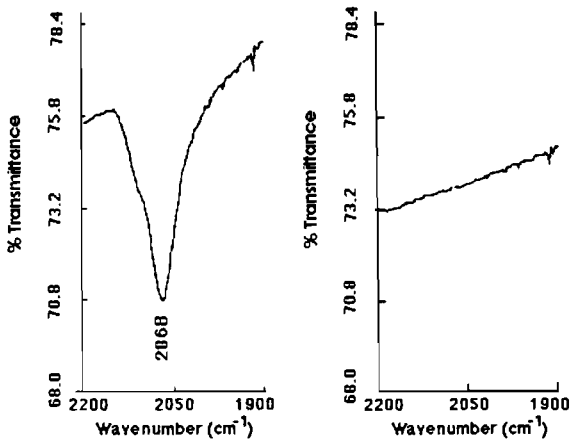

Figure 3. Diffuse reflectance FTIR spectra of the electrode surface after irradiation in 0.1 M $NaNO_3$ solution: (a) masked area; (b) irradiated area.

Table 1. Diffuse Reflectance FTIR Data of Photolyzed Electrode Surface in the Cyanide Stretching Frequency Range

M^{n+} incorporated	ν_{CN} in Masked Area (cm^{-1})	ν_{CN} in irradiated area (cm^{-1})	lit. value of ν_{CN} of $[MFe(CN)_6]^{2-}$ (cm^{-1})
Ni^{2+}	2072	2089	2087[15]
Fe^{2+}	2072	2082	2085,[16] 2081±1[17]
Cr^{3+}	2073	2093	2095,[16] 2092[18]
Mn^{2+}	2075	2063	2065[16]

However, when transition metal cations are present in the solution in which the electrode is photolyzed, mixed metal cyanometalate covers the irradiated areas after photolysis. We postulate the reaction to occur as follows. The photoinduced charge transfer reaction occurs as in solution, generating 2 mol of Fe(III) complex and 1 mol of Pt(II) complex.[13] Since the Pt complex is not coordinatively bound, it diffuses into the bulk solution. The Fe(III) complex reacts rapidly with transition metal cations in the interfacial region, forming an insoluble mixed metal cyanometalate which precipitates on the electrode surface.[15] The formation of these mixed metal cyanometalates is evidenced by diffuse reflectance FTIR data (Table 1). The cyanide stretching frequency was consistently around 2073 cm^{-1} in the masked areas. The broad feature of the band and the presence of shoulders indicate that this band is due to the presence of both terminal and bridging CNs in the film. On the other hand, in the irradiated areas, ν_{CN} varies with the incorporated transition metal cation but agrees reasonably well with the literature values[15-18] of ν_{CN} of ferrocyanides in the presence of their respective outer cations.

Electrochemical Studies of Multicomponent Films. The cyclic voltammograms of the Ni^{2+}-incorporated and the Fe^{2+}-incorporated electrodes are shown in Figure 4. In the case of Ni^{2+} (Figure 4a), a wave at 0.30 V vs SCE, the reported redox potential[19] for $[NiFe(CN)_6]^{2-/1-}$, was not present before irradiation; however, it was observed after photolysis, indicating the formation of nickel ferrocyanide on the irradiated surface. The peak current scan rate dependence reveals a linear relationship, indicating that the $[NiFe(CN)_6]^{2-/1-}$ is a surface-confined

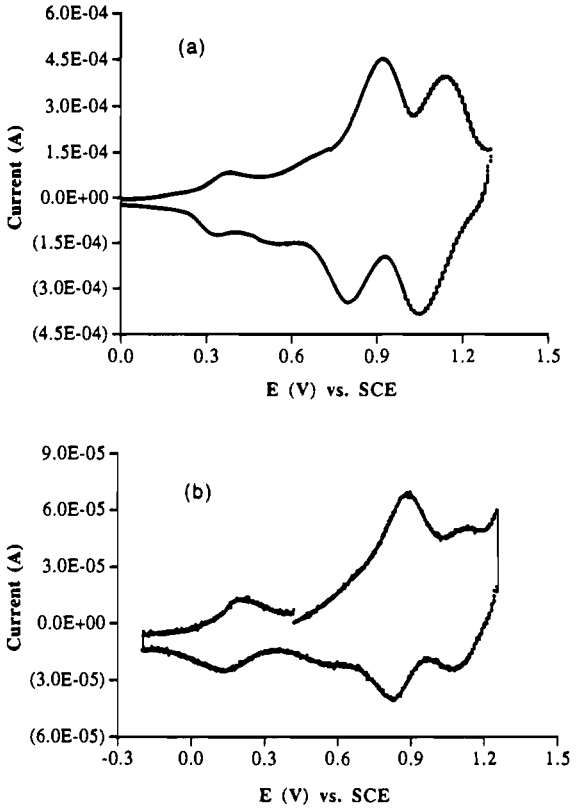

Figure 4. Cyclic voltammograms of a photolyzed electrode. Supporting electrolyte, 1.0 M $NaNO_3$; scan rate, 20 mV/s. (a) Ni^{2+} incorporated. The peak at 0.33 V corresponds to the redox event of nickel ferrocyanide. (b) Fe^{2+} incorporated. The peaks at 0.23 and 0.89 V are characteristic of the redox reactions of Prussian blue.

species. Similarly, in the Fe^{2+} case, cyclic voltammetric waves at 0.25 and 0.90 V vs SCE, characteristic of Prussian blue (PB), were observed upon photolysis. The characteristic blue color of the photolyzed regions further confirms the formation of PB.

Electron Probe Microanalysis. Detailed analysis of near-surface composition was carried out using the EPMA technique described in the Experimental Section. A typical backscattered electron micrograph is shown in Figure 5. Due to the fact that the backscattered electron signal scales with increasing atomic number, the brighter areas of the image correspond to higher Pt concentration. The large horizontal stripes correspond to the lines on the mask (50 lines per inch), while the smaller vertical stripes within a horizontal stripe are the result of a fortuitous diffraction pattern generated when monochromatic light was passed through the glass mask. It can be seen that the pattern on the electrode is strictly dependent on the photochemistry of the underlying polymer film.

The quantitative analysis of Pt and the incorporated metal dication across the horizontal bands, as well as along one of the dark bands (Pt poor), reveals periodic changes in the concentrations. A detailed line scan with 100 points at 10 μm intervals across the major bands and 250 points at 4 μm intervals along a dark band was performed for the Ni-incorporated surface, and the results are graphed in Figure 5. Data for the other transition metal cations which were also photochemically inserted are listed in Table 2. Line scan profiles show a rather constant concentration of Fe composition across the electrode, but a significant decrease in Pt concentration and an increase in M^{n+} (M = Ni in Figure 5) concentration in the photolyzed areas were observed, generating a periodic concentration profile which mimics the photolysis map. This again confirms that the incorporation of M^{n+} takes place only after the photodissociation of the original polymer film. By this process, two

(15) Sinha, S.; Humphrey, B. D.; Bocarsly, A. B. *Inorg. Chem.* **1984**, *23*, 203-212.
(16) Bertran, J. F.; Reguera-Ruiz, E.; Pasual, J. B. *Spectrochim. Acta. Part A* **1990**, *46A*, 1679-82.
(17) Wilde, R. E.; Ghosh, S. N.; Marshal, B. J. *Inorg. Chem.* **1970**, *9*, 2513.
(18) Shriver, D. F.; Shriver, S. A.; Anderson, S. E. *Inorg. Chem.* **1965**, *4*, 725.
(19) Humphrey, B. D.; Sinha, S.; Bocarsly, A. B. *J. Phys. Chem.* **1984**, *88*, 736-743.

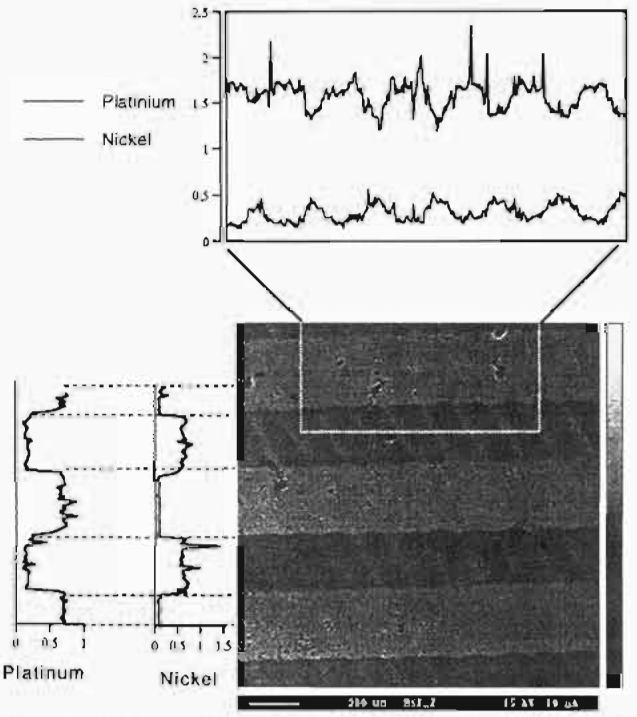

Figure 5. Backscattered electron-generated image of a stripe electrode surface. This specific polymer film was prepared by irradiating the derivatized electrode in a solution of 0.1 M $NiSO_4$. Dark stripes are the areas masked and represent Ni-rich/Pt-poor zones. The light stripes are the areas photolyzed and represent Ni-poor/Pt-rich zones.

Table 2. Electron Microprobe Data Indicating Relative Fractional Atomic Abundances in the Indicated Areas[a]

M^{n+}	masked area Pt M^{n+}	irradiated area Pt M^{n+}
Ni^{2+}	0.721	0.136
	0.094	0.693
Fe^{2+}	0.256	0.160
	0.996	1.211
Cr^{3+}	0.499	0.186
	0.039	0.268
Mn^{2+}	0.366	0.138
	0.024	0.168

[a] Each value reported is the average of at least three randomly chosen locations within each area. The unreported mass (to yield 100% total mass) resides in the light elements which form the ligands.

regions with distinctive redox properties are created on the electrode surface. Moreover, the structural control can be easily achieved by employing a masking technique or projecting a diffraction pattern onto the electrode surface.

An Electrochromic Diffraction Grating. When the polymer-derivatized electrode was irradiated in a solution of 0.1 M $Fe(NH_4)_2(SO_4)_2$, Fe^{2+} was incorporated into the ferricyanide lattice, forming Prussian blue (PB) on the irradiated surface and giving rise to an electrode surface with alternating blue and light yellow stripes.

When the beam of a He−Ne laser (633 nm) is passed through the electrode, the patterned surface acts as a diffraction grating. Red light is absorbed by PB due to its intervalence charge transfer centered at 710 nm, while the $[Fe-Pt]_n$ film is transparent in this spectral region. A radiometer was used to measure light intensity along the diffraction pattern with the result shown in Figure 6. Diffraction out to the fifth-order bands is clearly visible. The stripe spacing calculated on the basis of the diffraction pattern is 0.253 mm, in good agreement with the band width on the mask (0.245 mm) and the width measured

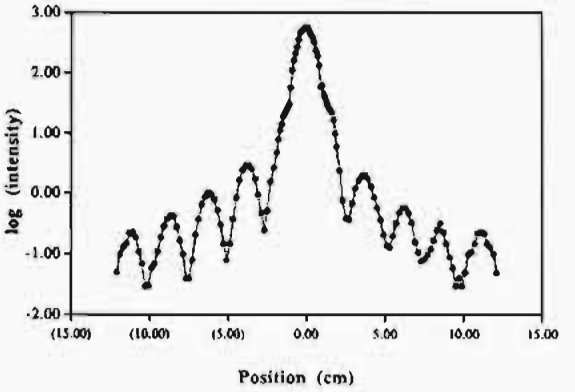

Figure 6. Light intensity along the diffraction pattern generated from a beam of 633 nm light passed through an electrode with a PB-striped surface.

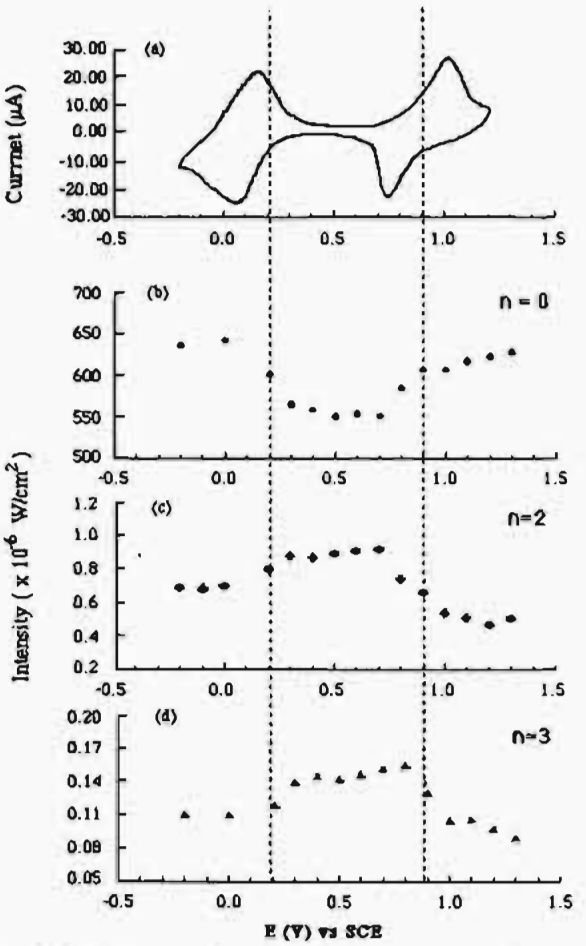

Figure 7. Light intensity along the diffraction pattern as a function of applied electrode potential: (a) cyclic voltammogram of Prussian blue derivatized on an ITO surface; (b) light intensity monitored at the $n = 0$ position of the diffraction pattern; (c) light intensity monitored at $n = 2$; (d) light intensity monitored at $n = 3$.

from the electron probe micrograph (0.252 mm). The interesting feature of this diffraction grating is that it can be turned "on" and "off" by controlling the potential of the derivatized electrode. Iron(III) hexacyanoferrate(II) appears blue in the potential range of 0.25 to 0.90 V vs SCE.[20] When the applied bias is such that all Fe centers in PB are in either the 2+ oxidation state or the 3+ oxidation state, it no longer has an intervalence electron transfer and thus does not absorb in the

(20) Roig, A.; Navarro, J.; Garcia, J. J.; Vicente, F. *Electrochim. Acta* **1994**, *39*, 437−442.

red. As a result, outside the 0.25−0.90 V vs SCE potential window, the entire electrode surface becomes transparent to red light, and the diffraction pattern disappears. Visually, the blue stripes on the electrode surface fade away. Figure 7 shows the dynamic response of the grating upon varying the potential as observed at $n = 0$, 2, and 3 diffraction features ($n = 1$ was too close to $n = 0$ to ensure accurate intensity measurements). As the electrode potential moves toward the region of 0.25 to 0.9 V vs SCE, the light intensity at $n = 2$ and $n = 3$ increases due to enhanced light diffraction. Outside the specified potential window, no diffraction pattern is clearly observable.

Repeated cycling of the working electrode potential showed that the electrode maintained good reversibility. Color changes were noted after more than 100 cycles, and the switching action of the electrode was still operative after 2 months. No specific storing conditions were applied. The clear diffraction pattern obtained serves to prove that no significant diffusion of chemical species between adjacent chemical regions has taken place even after prolonged times.

Conclusion

In summary, chemically modified electrodes with a coordination polymer-based two-component lateral mesostructure are easily obtained by the above-reported single-step photochemical process. Good uniformity and stability of the film was achieved by utilizing the robust chemical nature of the cyanometalates. Structures of this type offer opportunities in terms of dynamic photonic components.

Acknowledgment. This work was supported by the National Science Foundation under Grant No. CHE9312056. The surface analysis work made use of Princeton Materials Institute's MRSEC Shared Facilities supported by the National Science Foundation under Award No. DMR-940032. Acknowledgments are also extended to Ms. Stefanie Sharp for preparing complex **A** used in this study and Dr. Christopher Warren for helpful contributions toward the development of the polymerization electrochemistry and photochemistry.

IC941450T